Supporting Information

Efficient Removal of Pb(II) and Cd(II) from Industrial Mine Water by a Hierarchical MoS_2/SH-MWCNT Nanocomposite

Rashi Gusain[a,b*], Neeraj Kumar[a], Elvis Fosso-Kankeu[c] and Suprakas Sinha Ray[a,b*]

[a]DST-CSIR National Centre for Nanostructured Materials, Council for Scientific and Industrial Research, Pretoria 0001, South Africa.
[b]Department of Applied Chemistry, University of Johannesburg, Doornfontein 2028, Johannesburg, South Africa
[c]Water Pollution Monitoring and Remediation Initiatives Research Group, School of Chemical and Minerals Engineering, North West University, P. Bag X6001 Potchefstroom 2520, South Africa.

AUTHOR INFORMATION

Corresponding Authors

*E-mail: dr.rashi20@gmail.com (R.G.)

*E-mail: rsuprakas@csir.co.za, ssinharay@uj.ac.za (S.S.R.)

ORCID

Rashi Gusain: 0000-0002-7340-7237

Neeraj Kumar: 0000-0001-5019-6329

Elvis Fosso-Kankeu: 0000-0002-7710-4401

Suprakas Sinha Ray: 0000-0002-0007-2595

Characterization. To investigate the crystallinity and phase purity of MoS_2/SH-MWCNT nanocomposite and other intermediate products, powder X-ray diffraction (XRD) analysis was performed using a PANalytical X' Pert Pro diffractometer operated at 45 kV and 40 mA. All diffractograms were recorded from 5° to 90° 2θ range with Cu Kα radiation as the X-ray source at 1.54 Å wavelength. To probe the developed functional groups on the MWCNT and functionalization with MoS_2, Fourier transform infrared spectroscopy (FTIR) and X-ray photoelectron spectroscopy (XPS) were performed. Raman analysis of as prepared samples was performed on Alpha 300RAS Plus confocal micro-Raman spectrometer (WiTec Focus Innovations, Germany) operated at 5.0 mW laser power (ʎ = 532 nm excitation) using a 50X magnified lens. FTIR analysis for all samples was

performed on a Perkin-Elmer, USA (Spectrum 100) using KBr pellets on absorption mode at a resolution of 4 cm^{-1} in the range of 400 – 4000 cm^{-1}. X-ray photoelectron spectroscopy (XPS) was conducted on Kratos Axis Ultra device (Kratos, UK) electron spectrophotometer using Al Kα excitation radiation source. Morphological distribution of MoS_2 nanosheets on MWCNTs was well characterized using a Field Emission-Scanning Electron Microscope (Auriga FESEM, Carl Zeiss, Germany). An energy dispersive X-ray spectrometer (EDS, Oxford, UK), coupled with FESEM, was employed to analyze the elemental composition on the surfaces of nanocomposites. High resolution morphological and structural characterizations of MoS_2/SH-MWCNT nanocomposites were further performed using JEOL, 2100-JEM Japan High Resolution Transmission Scanning Electron Microscope (HRTEM), at 200 kV voltage, coupled with an EDS (Thermo Scientific, USA). The specific surface area and porosity of the MoS_2-SH-MWCNT nanocomposite was examined by Multi-Point Brunauer–Emmett–Teller (BET) analysis on running Nitrogen adsorption/desorption isotherms on a Micromeritics (ASAP 2020, USA) surface area analyzer.

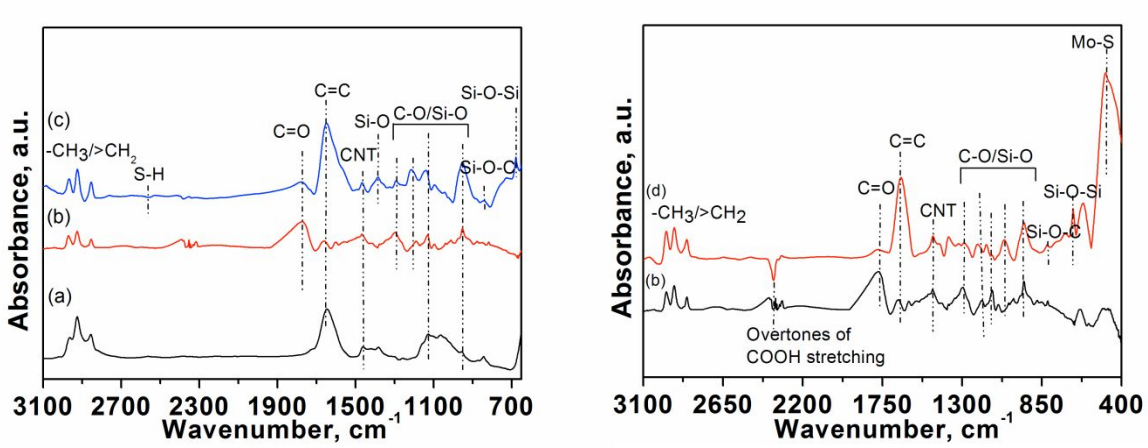

Figure S1. FTIR spectra of (a) MWCNTs, (b) oxidized MWCNTs (O-MWCNTs), (c) thiol functionalized MWCNTs (SH-MWCNTs), and (d) MoS_2/SH-MWCNT nanocomposite.

Figure S1 compares the functional groups noticed using FTIR spectroscopy, present on MWCNT, O-MWCNT, SH-MWCNT, and MoS_2/SH-MWCNT nanocomposite. All MWCNT nanocomposite exhibit vibrational signals at 2960–2950 cm^{-1} which are assigned to the methyl and methylene (-C-H) symmetric and asymmetric stretching modes located at the defect sites on the MWCNTs sidewalls. In addition, the occurrence of the peak at 1460 cm^{-1} in all FTIR spectra is a characteristic of carbon

nanotubes.[1] Other vibrational peaks at 1650, 1160, and 1130-1000 cm^{-1} present in all FTIR spectra are attributed to the C=C, symmetric C-O, and asymmetric C-O stretching modes, respectively. The reduced intensity of methyl and methylene (-C-H) symmetric and asymmetric stretching modes in O-MWCNTs suggest the existence of other functional groups at the defect sites during oxidation of MWCNTs.[2] O-MWCNTs also comprise other additional vibrational signatures when compared with pristine MWCNTs which again confirms the occurrence of functional groups (such as carboxylic groups, hydroxyl groups) after oxidation. Vibrational peaks at around 2350 cm^{-1} might be due to the presence of –C=C=O, -N=C=O, and -C≡N groups and overtones of C-O.[3] The appearance of a new peak at 1770 cm^{-1} after oxidation of MWCNTs might be due to the introduction of carboxylic groups (-COOH). On functionalization of O-MWCNTs with MPES, the reduced intensity of the peak at 1770 cm^{-1} and the presence of additional peaks suggests the formation of SH-MWCNTs. Vibrational signatures in the FTIR spectrum of SH-MWCNTs at 1280-1000, 841, and 675 cm^{-1} are assigned to the Si-O along with C-O, Si-O-Si, and Si-O-C stretching, respectively. Furthermore, the weak signature at 2561 cm^{-1} is due to S-H stretching which confirms the presence of a thiol functional group in SH-MWCNTs.[4] MoS_2/SH-MWCNT nanocomposite depict a typical MoS_2 vibrational peak at 489 cm^{-1} among other well characterized peaks of MWCNTs, which proves the successful synthesis of MoS_2 nanosheets on the thiol functionalized MWCNTs.

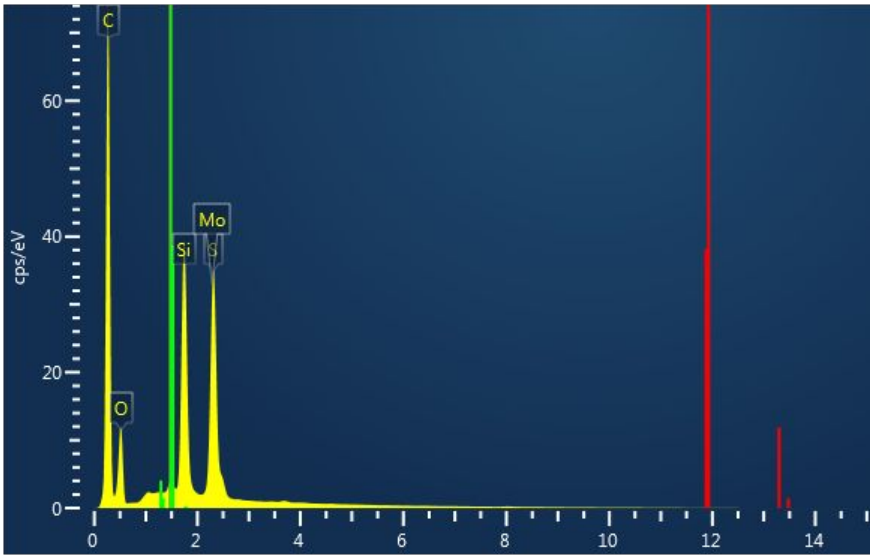

Figure S2. EDX spectrum of MoS_2/SH-MWCNT nanocomposite

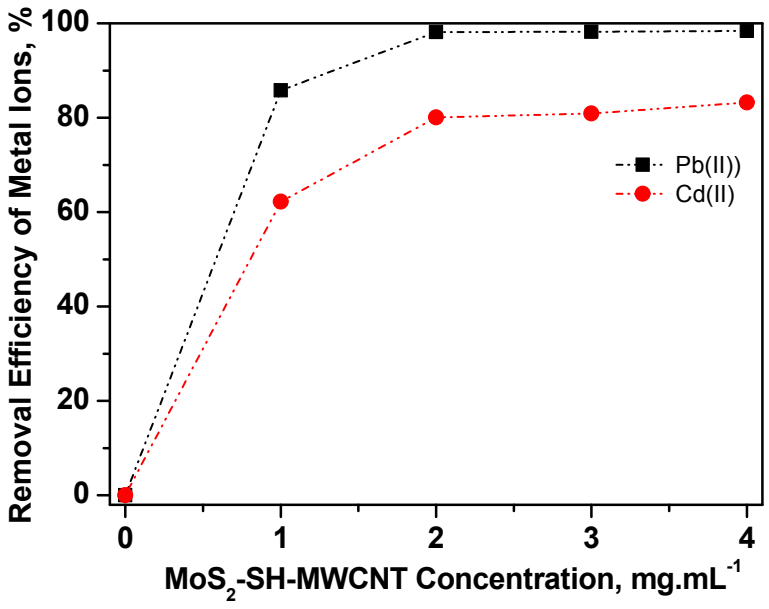

Figure S3. Percentage of heavy metal (Pb(II) and Cd(II)) removal from mine water on using different doses of MoS_2/SH-MWCNT nanocomposites. Adsorption conditions: heavy metal concentration (C_o): 100 mg. L^{-1}, temperature = 25 °C, and time = 60 min.

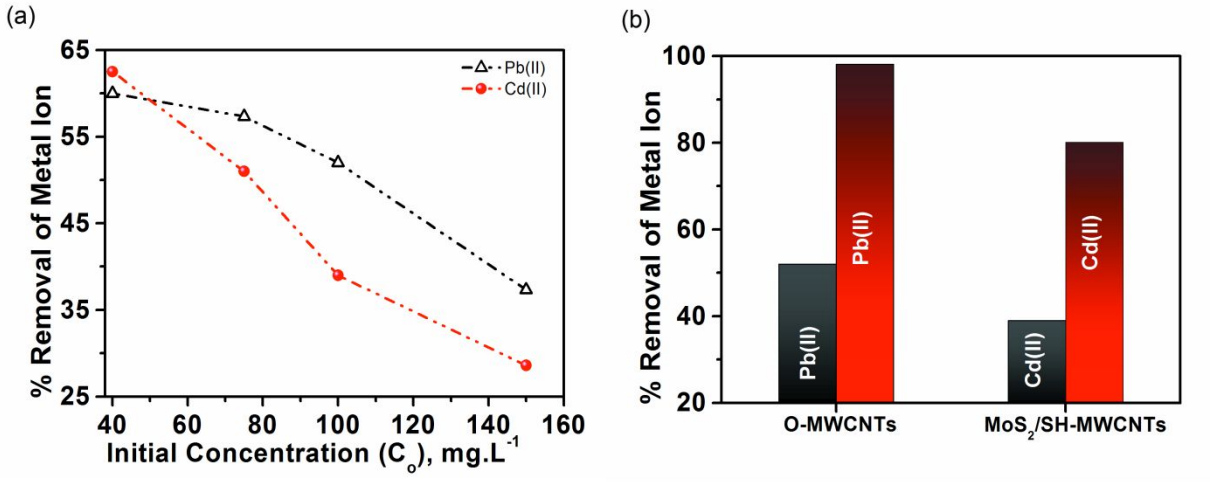

Figure S4. (a) Percentage of heavy metal for different initial concentrations of Pb(II) and Cd(II) removal from mine water using 2 $mg.mL^{-1}$ O-MWCNTs. (b) Comparison of % removal of Pb(II) and Cd(II) (100 $mg.L^{-1}$) using 2 $mg.mL^{-1}$ O-MWCNT and MoS_2/SH-MWCNT nanocomposites.

Temkin Adsorption Isotherm. Temkin isotherm is generally expressed for heterogeneous adsorbent surface energy systems with nonuniform distribution of heat of sorption. The Temkin isotherm can be expressed using equation 1:

$$Q_e = \beta\, LnA_T + \beta\, LnC_e \quad \text{(S1)}$$

where Q_e and C_e are amount of adsorbate adsorbed ($mg.g^{-1}$) and remaining concentration of adsorbate in solution ($mg.L^{-1}$) at equilibrium, β and AT are the constant related to heat of sorption ($J.mol^{-1}$) and Temkin isotherm equilibrium constant ($L.g^{-1}$), respectively.

Temkin isotherm constant (b) can also be calculated with the help of the β value from equation S1 as expressed in equation S2:

$$\beta = \frac{RT}{b} \quad \text{(S2)}$$

where R is the universal gas constant (8.314 $J.mol^{-1}.K^{-1}$), and T stands for temperature (K).

The Temkin isotherm can be obtained by plotting a graph of Q_e versus LnC_e (Figure SI4)

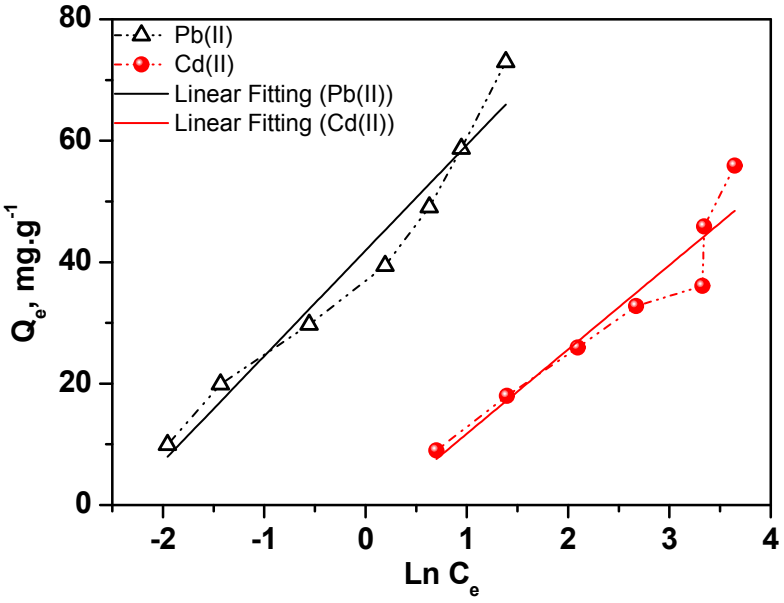

Figure SI5. Temkin adsorption isotherm plot for Pb(II) and Cd(II) adsorption from mine water using MoS_2/SH-MWCNT nanocomposite. Adsorption conditions: time = 60 min, temperature = 25 °C, and adsorbent dosage = 2 $mg.mL^{-1}$.

Dubinin-Radushkevich (D-R) Adsorption Isotherm. D-R adsorption isotherm is expressed to describe the adsorption on porous materials. A linear equation of D-R isotherm is given in equation S3:

$$LnQ_e = LnQ_s \; - \; K_{ad}.\varepsilon^2 \qquad \text{(S3)}$$

where Q_s, ε, and K_{ad} are the theoretical saturation capacity ($mg.g^{-1}$), polanyi potential, and D-R adsorption isotherm constant ($mol^2.J^{-2}$), respectively.

The value of ε can easily be calculated using the following equation:

$$\varepsilon = RT\ Ln\ (1 + \frac{1}{C_e}) \qquad \text{(S4)}$$

In addition, with the help of the value of K_{ad}, the value of mean free energy of adsorption (E) can easily be calculated using equation S5:

$$E = \frac{1}{\sqrt{2K_{ad}}} \qquad \text{(S5)}$$

Figure S6 presents the D-R isotherm linear plot (Ln Q_e versus ε^2) for heavy metal adsorption.

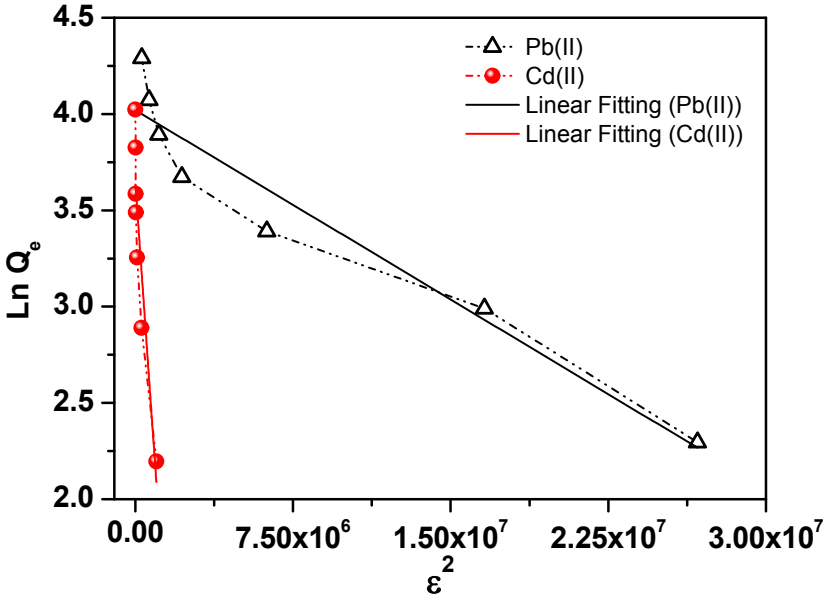

Figure S6. D-R adsorption isotherm plot for Pb(II) and Cd(II) adsorption from mine water using MoS_2/SH-MWCNT nanocomposite. Adsorption conditions: time = 60 min, temperature = 25 °C, and adsorbent dosage = 2 $mg.mL^{-1}$.

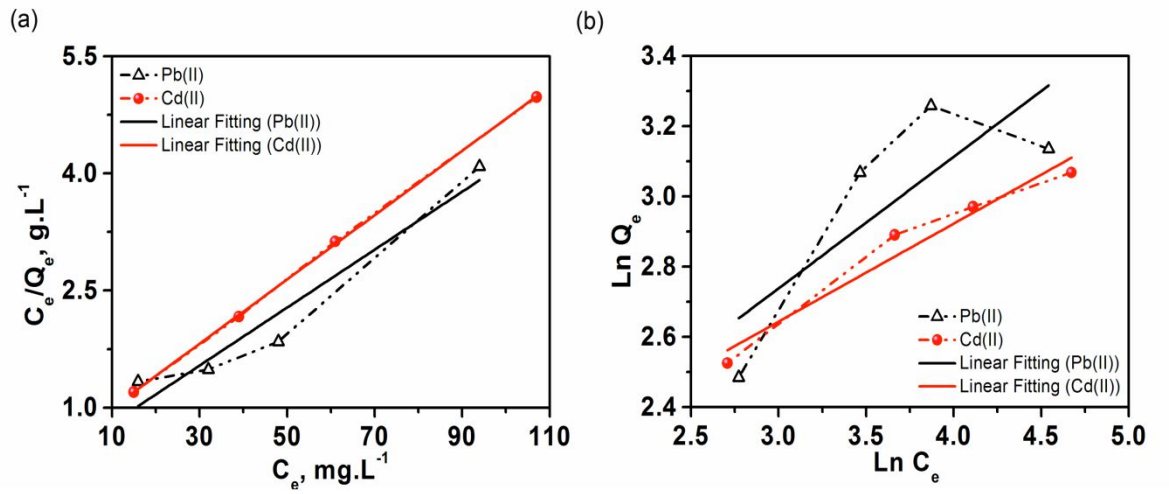

Figure S7. (a) Langmuir and (b) Freundlich adsorption isotherms for Pb(II) and Cd(II) adsorption using O-MWCNTs. Adsorption conditions: time = 60 min, temperature = 25 °C, adsorbent dosage = 2 mg.mL^{-1}.

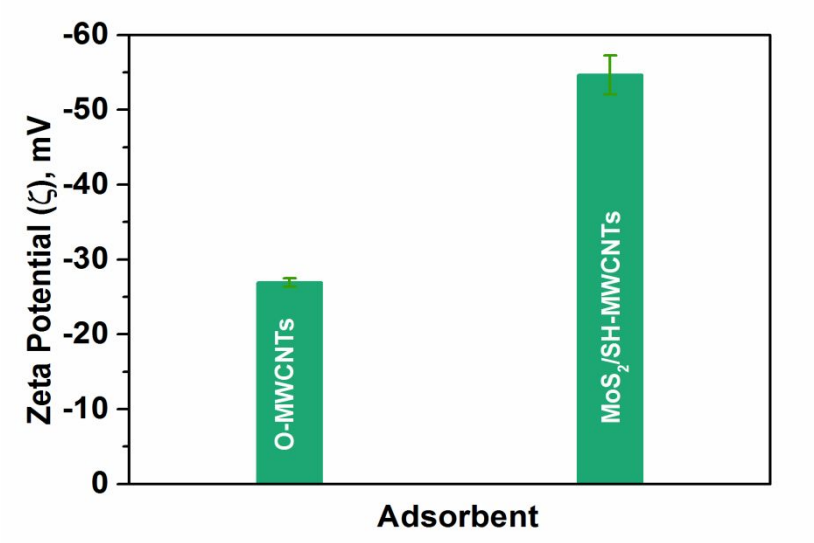

Figure S8. Zeta potential of O-MWCNTs and MoS_2/SH-MWCNTs nanocomposite.

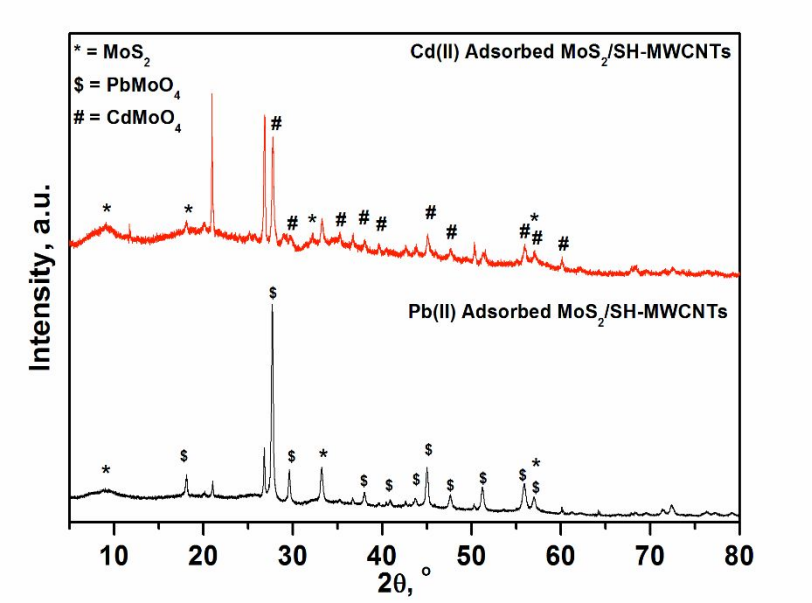

Figure S9. XRD of MoS_2/SH-MWCNT nanocomposite after adsorption of Pb(II) and Cd(II) from mine water. * represents MoS_2, $ represents $PbMoO_4$, and # represents $CdMoO_4$ lattice planes.

Table S1. Physical properties and cation and anion concentration present in mine water

Physical parameters	**pH**	**Electrical Conductivity**	**Total Alkalinity**	**Chemical Oxygen Demand**	**Turbidity**
Parameter Value	6.0	0.1 $mS.m^{-1}$	5 $mg.L^{-1}$	10 $mg.L^{-1}$	0.1 NTU

Cations	**Zn**	**Ni**	**Mn**	**Pb**	**Fe**	**Cu**	**Cr**
Concentration, $mg.L^{-1}$	0.025	0.025	0.025	0.01	0.025	0.025	0.025
Cations	**Co**	**Cd**	**Al**	**Mg**	**Ca**	**K**	**Na**
Concentration, $mg.L^{-1}$	0.025	0.003	0.1	2.0	2.0	1.0	2.0

Anions	**F**	**Cl**	**Phosphate**	**Sulphate**	**Nitrate**	**Nitrite**	**NH_3**
Concentration, $mg.L^{-1}$	0.2	20	0.1	2	0.1	0.05	0.1

Table S2. Values of kinetic parameters for Pb(II) and Cd(II) from mine water using MoS_2/SH-MWCNTs nanocomposite

Kinetic Model	Parameters	Pb (II)	Cd(II)
		Parameter Value	
Pseudo First Order Kinetics	R^2	0.77	0.85
	k_1	0.041	0.054
	Q_e(cal)	11.43	11.02
Pseudo Second Order Kinetics	R^2	0.99	0.99
	k_2	0.014	0.018
	$Q_{e(cal)}$	50	40
	$Q_{e(exp)}$	49.06	36.1
Intraparticle Diffusion	R^2	0.78	0.70
	k_{id}	0.47	0.45

Table S3. Equation and parameter values of adsorption isotherms for Pb(II) and Cd(II) from mine water using MoS_2/SH-MWCNTs nanocomposite

Isotherm	Linear Equation	Parameters	Pb(II)	Cd(II)
			Parameter Value	
Langmuir	$\frac{C_e}{Q_e} = \frac{1}{K_L . Q_m} + \frac{C_e}{Q_m}$	R^2	0.95	0.87
		Q_m	90	66.6
		K_L	0.825	0.75
Freundlich	$Ln\ Q_e = \frac{1}{n} Ln\ C_e + Ln\ K_f$	R^2	0.96	0.94
		K_f	35.87	7.27
		1/n	0.544	0.546
Temkin	$Q_e = \beta\ LnA_T + \beta\ LnC_e$	R^2	0.952	0.899
		β	17.4	13.88
		A_T	10.54	0.857
Dubinin-Radushkevitch (D-R)	$LnQ_e = LnQ_s - K_{ad}.\varepsilon^2$	R^2	0.85	0.675
		K_{ad}	0.70	15.84
		Q_s	2.16	19.668

REFERENCES

(1) Misra, A.; Tyagi, P. K.; Rai, P.; Misra, D., FTIR spectroscopy of multiwalled carbon nanotubes: a simple approachto study the nitrogen doping. *Journal of nanoscience and nanotechnology* **2007,** *7* (6), 1820-1823.

(2) Zhang, J.; Zou, H.; Qing, Q.; Yang, Y.; Li, Q.; Liu, Z.; Guo, X.; Du, Z., Effect of Chemical Oxidation on the Structure of Single-Walled Carbon Nanotubes. *The Journal of Physical Chemistry B* **2003,** *107* (16), 3712-3718.

(3) Saleh, T. A.; Agarwal, S.; Gupta, V. K., Synthesis of MWCNT/MnO2 and their application for simultaneous oxidation of arsenite and sorption of arsenate. *Applied Catalysis B: Environmental* **2011,** *106* (1), 46-53.

(4) Zhou, S.; Zhou, X.; Jiang, W.; Wang, T.; Zhang, N.; Lu, Y.; Yu, L.; Yin, Z., (3-Mercaptopropyl)trimethoxysilane-Assisted Synthesis of Macro- and Mesoporous Graphene Aerogels Exhibiting Robust Superhydrophobicity and Exceptional Thermal Stability. *Industrial & Engineering Chemistry Research* **2016,** *55* (4), 948-953